Cell

Osh Proteins Regulate Phosphoinositide Metabolism at ER-Plasma Membrane Contact Sites

Christopher J. Stefan,[1,2] Andrew G. Manford,[1,2] Daniel Baird,[1,3] Jason Yamada-Hanff,[1,4] Yuxin Mao,[1] and Scott D. Emr[1,*]
[1]Weill Institute for Cell & Molecular Biology, Department of Molecular Biology & Genetics, Cornell University, Ithaca, NY 14853, USA
[2]These authors contributed equally to this work
[3]Present address: Novartis Institutes for Biomedical Research, 250 Massachusetts Avenue, Cambridge, MA 02139, USA
[4]Present address: Program in Neuroscience, Harvard Medical School, 220 Longwood Avenue, Boston, MA 02215, USA
*Correspondence: sde26@cornell.edu
DOI 10.1016/j.cell.2010.12.034

SUMMARY

Sac1 phosphoinositide (PI) phosphatases are essential regulators of PI-signaling networks. Yeast Sac1, an integral endoplasmic reticulum (ER) membrane protein, controls PI4P levels at the ER, Golgi, and plasma membrane (PM). Whether Sac1 can act in *trans* and turn over PI4P at the Golgi and PM from the ER remains a paradox. We find that Sac1-mediated PI4P metabolism requires the *o*xysterol-binding *h*omology (Osh) proteins. The PH domain-containing family member, Osh3, localizes to PM/ER membrane contact sites dependent upon PM PI4P levels. We reconstitute Osh protein-stimulated Sac1 PI phosphatase activity in vitro. We also show that the ER membrane VAP proteins, Scs2/Scs22, control PM PI4P levels and Sac1 activity in vitro. We propose that Osh3 functions at ER/PM contact sites as both a sensor of PM PI4P and an activator of the ER Sac1 phosphatase. Our findings further suggest that the conserved Osh proteins control PI metabolism at additional membrane contact sites.

INTRODUCTION

Phosphatidylinositol 4-phosphate, PI4P, serves as an essential signaling molecule at the plasma membrane (PM) and Golgi in the control of membrane trafficking, cytoskeletal organization, lipid metabolism, and signal transduction pathways (D'Angelo et al., 2008). Maintaining the proper balance of PI4P levels through the regulation of phosphoinositide (PI) kinases and phosphatases is critical. Sac1-like PI phosphatases are important regulators of PI4P turnover and are implicated in disease (Liu and Bankaitis, 2010). Yeast cells lacking Sac1 display elevated PI4P levels resulting in impaired membrane trafficking, abnormal vacuolar morphology, altered lipid metabolism, and growth defects (Foti et al., 2001; Guo et al., 1999; Rivas et al., 1999). Inactivation of Sac1 PI phosphatase activity provided by Sac1 and the synaptojanin-like proteins, Sjl2 and Sjl3, results in massive PI4P accumulation, secretory defects, and lethality (Foti et al., 2001). In mammalian cells, depletion of Sac1 leads to elevated cellular PI4P levels, Golgi fragmentation, and defects in mitotic spindle organization (Liu et al., 2008). Loss of Sac1 in the mouse and *Drosophila* results in embryonic lethality (Liu et al., 2008; Wei et al., 2003). Thus, Sac1 PI phosphatases are essential for multiple, conserved cellular functions.

Although Sac1 PI phosphatases are key modulators of PI4P metabolism, little is known about their regulation. Both yeast and mammalian Sac1 are integral membrane proteins localized to the endoplasmic reticulum (ER) and Golgi (Faulhammer et al., 2007; Foti et al., 2001; Nemoto et al., 2000). Upon starvation in yeast, or in the absence of growth factors in mammalian cells, Sac1 traffics from the ER to the Golgi where it antagonizes PI4P synthesis and Golgi function (Blagoveshchenskaya et al., 2008; Faulhammer et al., 2007). Although roles for Sac1 in the control of PI4P pools at the ER and Golgi are known, less is understood about how Sac1 regulates PI4P levels at the PM. Previous studies indicate that *sac1*Δ mutant yeast cells accumulate PI4P at the PM generated by the PI 4-kinase Stt4 (Baird et al., 2008; Foti et al., 2001; Roy and Levine, 2004). Yet, Sac1 is not known to traffic to the PM, nor is it known if Sac1 regulates PM PI4P pools from the ER. A recent study describing the molecular structure of the Sac1 catalytic domain suggests that Sac1 may act in *trans* from the ER to turn over PI4P at the PM (Manford et al., 2010). However, factors that link Sac1 PI phosphatase activity to PI4P at the PM are unknown.

We find that PI4P metabolism and Sac1 function require the *o*xysterol-binding *h*omology (Osh) protein family. In particular, Osh3 assembles at cortical ER (cER) structures in response to PM PI4P levels. We reconstitute Osh protein-stimulated Sac1 PI phosphatase activity against PI4P-containing liposomes in vitro. In addition the ER membrane VAP proteins, Scs2 and Scs22, control PM PI4P levels in vivo and Sac1 activity in vitro. We propose that the Osh and VAP proteins regulate Sac1 PI phosphatase activity at PM/ER membrane contact sites. We also discuss potential roles for these proteins in the control of PI metabolism at additional membrane contact sites. Membrane junctions between the ER and other organelles are sites for lipid transfer and metabolism, Ca^{2+} transport and signaling, and the downregulation of insulin and growth factor receptors (reviewed

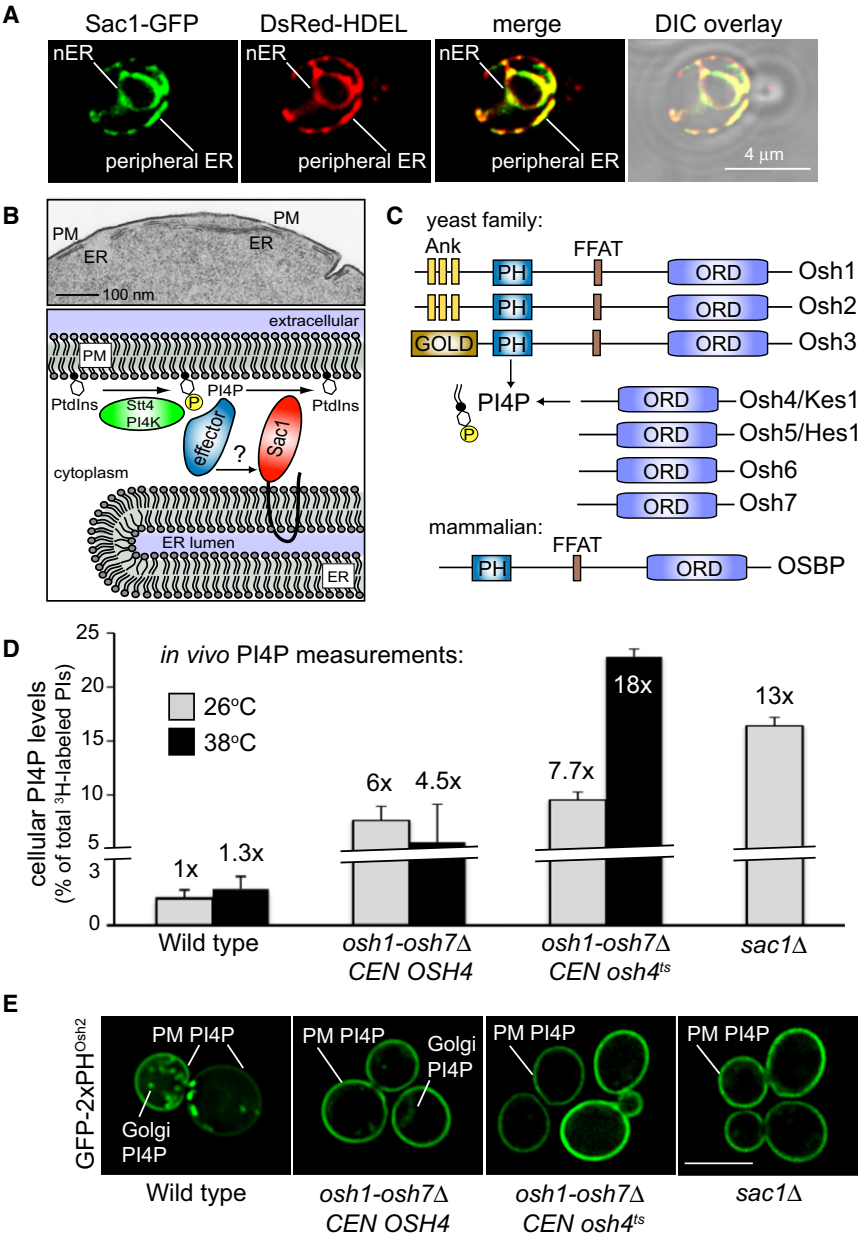

Figure 1. The Yeast OSBPs Control PI4P Metabolism

(A) Sac1-GFP localizes to the ER (marked by DsRed-HDEL). Peripheral ER and nuclear ER (nER) compartments are labeled. Scale bar, 4 μm. See also Figure S1B.

(B) Electron microscopy of a region of a yeast spheroplast showing proximity between cER and the PM (top, scale bar, 100 nm). Model for PI4P metabolism at PM/ER membrane contact sites (bottom).

(C) Diagram of the Osh proteins and OSBP. ORD, OSBP-related sterol-binding domain; FFAT, di-phenylalanines within an acidic track; PH, pleckstrin homology domain; GOLD, Golgi localization domain; Ank, ankyrin repeats.

(D) Cellular PI4P levels measured by ^{3}H-inositol labeling and HPLC analysis for wild-type, *osh*Δ [*CEN OSH4*], *osh*Δ [*CEN osh4^{ts}*], and *sac1*Δ cells at 26°C (gray) and 38°C (black). Error bars are the SD of three experiments. See also Figure S1C and Table S3.

(E) PI4P localization in wild-type, *osh*Δ [*CEN OSH4*], *osh*Δ [*CEN osh4^{ts}*], and *sac1*Δ cells. Wild-type, *osh*Δ [*CEN OSH4*], and *osh*Δ [*CEN osh4^{ts}*] cells carrying GFP-2xPH^{Osh2} were shifted to 38°C for 1 hr; *sac1*Δ cells were observed at 26°C. Scale bar, 4 μm.

in Lev, 2010). Thus, modulation of PI levels at membrane contact sites may provide a fundamental mechanism for signaling between cellular membrane compartments.

RESULTS

The Osh Proteins Regulate PI4P Metabolism

Yeast Sac1 is an integral membrane protein that localizes to nuclear and peripheral ER compartments (Figure 1A) (Foti et al., 2001). Yet, PI4P is generated by the PI 4-kinases Stt4 and Pik1 at the PM and the Golgi, respectively (Figure 1E) (Audhya et al., 2000). It is not known whether ER-embedded Sac1 turns over these distinct PI4P pools. Sac1 traffics between the ER and Golgi to regulate PI4P levels at these intracellular compartments (Faulhammer et al., 2007). However, to our knowledge, Sac1 has not been found at the PM. We reasoned that ER-localized Sac1 might control PM PI4P pools at PM/ER membrane contact sites where the peripheral ER closely apposes the PM (within 10 nm) (Figure 1B). Although Sac1 localizes to the peripheral ER (Figure 1A), no proteins that regulate Sac1 activity at PM/ER membrane contact sites are known.

We hypothesized that a PI4P effector might link PI4P at the PM to Sac1 at the ER (Figure 1B). For this we focused on the PI4P-binding proteins Osh1, Osh2, and Osh3, members of the *o*xysterol-binding protein *h*omology family (Figure 1C). Osh2 and Osh3 possess PH domains that bind PI4P and localize to cortical, punctate structures (Figure 1C, Figure 2A, and Figure S2 available online) (Levine and Munro, 2001; Roy and Levine, 2004). Osh1 also contains a PH domain but localizes to the Golgi and nuclear-vacuolar membrane junction sites (Levine and Munro, 2001). Osh1, Osh2, and Osh3 are similar to mammalian *o*xysterol-*b*inding *p*rotein (OSBP) that contains a PI4P-binding PH domain (Figure 1C). These proteins are members of the OSBP-related protein (ORP) family that contain sterol-binding *O*SBP-*r*elated *d*omains (ORDs) (Figure 1C). Among the ORP family, Osh4/Kes1 does not possess

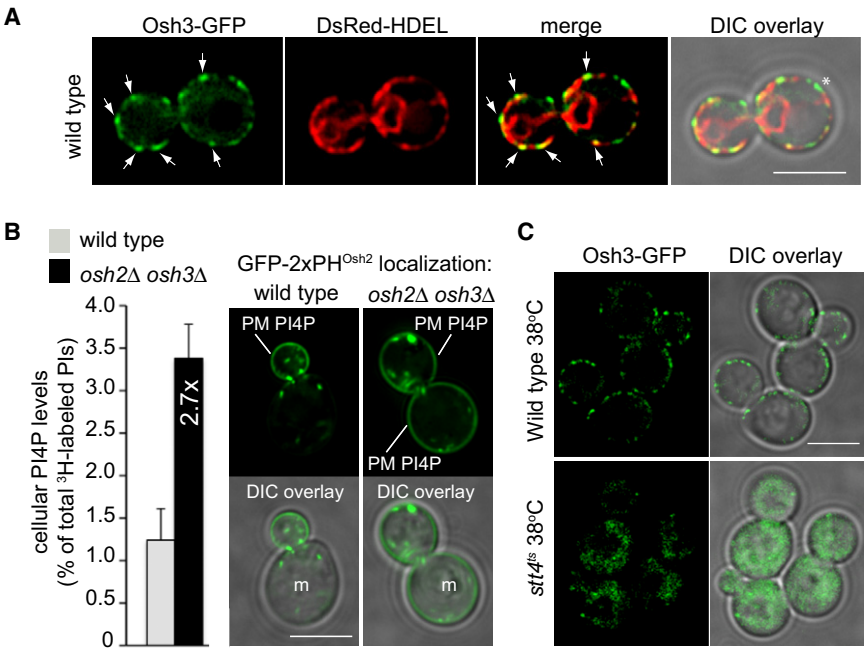

Figure 2. Osh2 and Osh3 Localize to PM/ER Contact Sites and Control PM PI4P

(A) Osh3-GFP localization in wild-type cells coexpressing the DsRed-HDEL ER marker. Arrows show Osh3-GFP puncta associated with cER. The asterisk shows an Osh3-GFP patch not associated with the cER. See also Figure S2A.

(B) Cellular PI4P levels in wild-type and *osh2*Δ *osh3*Δ mutant cells measured by ^{3}H-inositol labeling and HPLC analysis (left). Error bars are the SD of three experiments. See also Table S3. GFP-2xPH^{Osh2} (PI4P) localization in wild-type or *osh2*Δ *osh3*Δ mutant cells (right). Mother cells are indicated (m).

(C) Osh3-GFP localization in wild-type or *stt4*^{ts} cells at 38°C. Levels were enhanced using Adobe Photoshop in the DIC overlay image for *stt4* mutant cells (lower left). See also Figure S2B.

(D) Growth of *osh*Δ [*CEN osh4*^{ts}] cells coexpressing *OSH3* alleles. Serial dilutions of cells carrying empty vector or Osh3-GFP constructs were incubated at 26°C and 38°C. Osh3-GFP mutant constructs are indicated: AAAT, substitution of phenylalanines in the FFAT motif with alanine, ΔPH, deletion of the PH domain. See also Figure S2C. Scale bars, 4 μm.

a PH domain but also binds PI lipids (Figure 1C) (Li et al., 2002). Osh4/Kes1 is also known to regulate PI4P levels at the Golgi (Fairn et al., 2007; Li et al., 2002). Given the properties of the Osh protein family to bind PI4P, regulate PI4P (in the case of Osh4/Kes1), and to localize to membrane contact sites, we further examined the role of the Osh proteins in PI4P metabolism.

First, we measured PI4P levels in cells lacking Osh protein function. For this we utilized strains that lack the *OSH1-OSH7* genes and carry wild-type *OSH4* or a temperature-sensitive allele, *osh4-1*, on a plasmid because loss of all Osh proteins is lethal (*osh*Δ:*CEN OSH4* or *osh*Δ:*CEN osh4*^{ts} cells) (Beh and Rine, 2004). In ^{3}H-inositol labeling experiments, PI4P levels were 6- to 7-fold higher than wild-type cells in *osh*Δ:*CEN OSH4* and *osh*Δ:*CEN osh4*^{ts} cells at the permissive temperature (26°C) (Figure 1D), suggesting that Osh proteins (other than Osh4) control PI4P levels in vivo. At the restrictive temperature for *osh*Δ:*CEN osh4*^{ts} cells, PI4P levels were elevated 18-fold above wild-type levels (38°C) (Figure 1D) and were greater than PI4P levels in *sac1*Δ mutant cells (13-fold above wild-type) (Figure 1D). Expression levels of a Sac1-GFP fusion were slightly reduced in *osh*Δ:*CEN osh4*^{ts} mutant cells at 38°C (approximately 3-fold) (Figure S1A). This did not account for the 18-fold increase in PI4P in *osh*Δ:*CEN osh4*^{ts} cells because complete loss of Sac1 resulted in only a 13-fold increase in PI4P (*sac1*Δ cells) (Figure 1D). Moreover, GFP-Sac1 localized to both nuclear and peripheral ER compartments in wild-type and *osh*Δ:*CEN osh4*^{ts} cells at 38°C (Figure S1B). The 18-fold increase in PI4P levels in *osh*Δ:*CEN osh4*^{ts} mutant cells resembled levels previously reported for triple mutant *sac1*^{ts} *sjl2*Δ *sjl3*Δ cells (Foti et al., 2001), suggesting that the Osh proteins may regulate multiple Sac1-like PI phosphatase activities. We also examined PI4P levels in cells lacking both Sac1 and Osh protein function to test for additive effects. PI4P levels were not further elevated in *sac1*^{ts} *osh*Δ:*CEN osh4*^{ts} cells compared to *osh*Δ:*CEN osh4*^{ts} cells at 38°C (Figure S1C and Table S3), suggesting that Sac1 and the Osh proteins act in a common pathway. Together, these results implicate the Osh proteins in PI4P metabolism and Sac1 phosphatase function.

The PI4P FLARE (*f*luorescent *l*ipid-associated *re*porter) GFP-2xPH^{Osh2} is found at Golgi compartments and the PM via Pik1 and Stt4 PI 4-kinase activities, respectively, in wild-type cells (Figure 1E) (Roy and Levine, 2004). In contrast the PI4P FLARE was stabilized at the PM in *osh*Δ:*CEN OSH4* and *osh*Δ:*CEN osh4*^{ts} cells, although weak fluorescence at intracellular puncta was detected (Figure 1E). The PI4P FLARE was also increased at the PM in *sac1*Δ cells, consistent with elevated levels of Stt4-generated PI4P at the PM (Figure 1E) (Baird et al., 2008; Foti et al., 2001; Roy and Levine, 2004). Although previous studies have implicated one Osh family member, Osh4/Kes, in PI4P regulation at the Golgi

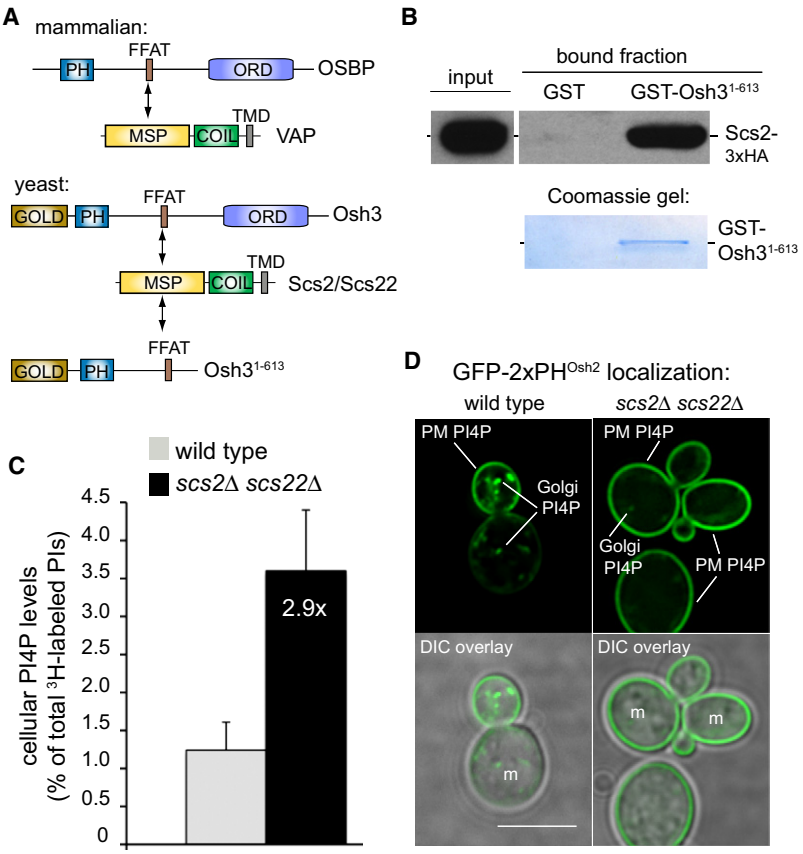

Figure 3. The VAP Proteins Scs2 and Scs22 Control PM PI4P Metabolism

(A) Diagrams of mammalian VAP, yeast Scs2/Scs22, OSBP, and Osh3. VAP proteins possess a *m*ajor sperm *p*rotein domain (MSP), a coiled-coil, and a transmembrane domain (TMD).

(B) The GST-Osh3$^{1–613}$ fusion binds Scs2-3xHA from solubilized yeast lysates. GST alone does not bind Scs2-3xHA. Total input and bound fractions are shown.

(C) Cellular PI4P levels in wild-type and *scs2*Δ *scs22*Δ cells measured by ^{3}H-inositol labeling and HPLC analysis. Error bars show SD of three independent experiments. See also Table S3.

(D) Localization of GFP-2xPH^{Osh2} (PI4P) in wild-type and *scs2*Δ*scs22*Δ cells. Mother cells are indicated (m). Scale bar, 4 μm. See also Figure S3.

(Fairn et al., 2007; Li et al., 2002), our results suggested that additional Osh proteins control PI4P metabolism at the PM.

Osh3 Localizes to PM/ER Contact Sites in a PI4P-Dependent Manner

Several lines implicated Osh2 and Osh3 in the control of PI4P metabolism at the PM. First, both bind PI4P and localize to cortical structures (Figure 1C, Figure 2A, and Figure S2A) (Levine and Munro, 2001; Roy and Levine, 2004; Schulz et al., 2009). Second, expression of *OSH2* or *OSH3* from a plasmid partially rescued the increased PI4P levels in *osh*Δ:*CEN osh4^{ts}* mutant cells at 38°C (from 18-fold above wild-type to 5- and 8-fold, respectively) (Table S3). Third, *osh2*Δ *osh3*Δ double mutant cells displayed elevated PI4P levels, as measured by ^{3}H-inositol labeling experiments (2.7-fold above wild-type) (Figure 2B and Table S3). Lastly, the PI4P FLARE was stabilized at the PM in *osh2*Δ *osh3*Δ double mutant cells (particularly in mother cells), compared to wild-type cells (Figure 2B).

We examined if Osh3 localized to PM/ER membrane contact sites in order to regulate PI4P at the PM. Osh3-GFP localized to cortical patches often associated with cER compartments marked with DsRed-HDEL (Figure 2A, arrows), as well as the PM stained with filipin (Figure S2A). To confirm that Osh3 patches associated with cER, we examined Osh3-GFP localization in cells lacking the reticulons Rtn1, Rtn2, and Yop1 because the cER displays expanded sheet-like structures in these mutant cells (Voeltz et al., 2006). Osh3-GFP patches clustered at cER compartments (marked with DsRed-HDEL) adjacent to the PM (stained with filipin) in *rtn1*Δ *rtn2*Δ *yop1*Δ triple mutant cells and was absent from regions lacking cER structures (Figure S2A). Together, our results suggested that Osh3 localizes to PM/ER membrane contact sites and modulates PM PI4P levels, possibly by regulation of cER-localized Sac1.

Osh3 localization did not always coincide with cER compartments (Figure 2A, asterisk), suggesting that its assembly at PM/ER membrane contact sites may be dynamic and progress in regulated stages. Thus, we tested if Osh3 localization and function required PM PI4P. Osh3-GFP localized diffusely in the cytoplasm in cells with impaired Stt4 PI 4-kinase activity (*stt4^{ts}* cells; Figure 2C), showing that Osh3 localization required PM PI4P synthesis. In contrast, Osh3-GFP was present at the PM in *pik1^{ts}* mutant cells impaired in PI4P synthesis at the Golgi, although Osh3 was observed at intracellular structures in these cells (Figure S2B). Likewise, Osh3-GFP localized to cortical patches in cells with reduced PI(4,5)P_2 levels (*mss4^{ts}* cells) (Figure S2B). A form of Osh3 lacking its PH domain (Osh3$^{\Delta PH}$-GFP) did not rescue the growth defects of *osh*Δ:*CEN osh4^{ts}* mutant cells at 38°C (Figure 2D). In addition, Osh3$^{\Delta PH}$-GFP displayed increased cytoplasmic localization, compared to wild-type Osh3-GFP (Figure S2C). Thus, the assembly of Osh3 at cortical patches required PM PI4P synthesis, consistent with its ability to bind PI4P and control PM PI4P levels.

Next, we asked if other regions in Osh3 play a role in its function. Osh3 contains an FFAT motif (di-phenylalanines within an acidic track) (Figures 1C, 2D, and 3A). FFAT motifs bind the MSP domains of the yeast ER membrane proteins Scs2 and Scs22, orthologs of the mammalian ER membrane VAP proteins (Figure 3A) (Kaiser et al., 2005; Loewen et al., 2003). A form of Osh3 bearing substitutions in the FFAT motif (Osh3^{AAAT}-GFP) partially rescued the growth defects of *osh*Δ:*CEN osh4^{ts}* cells at 38°C (Figure 2D) and assembled at cortical patches (Figure S2C). A previous study reported that a mutant form of Osh3 with substitutions in the FFAT motif was mislocalized from the cER (Loewen et al., 2003). However, this study used

a GFP-Osh3 fusion that required Scs2 overexpression to target to the cER. Consistent with this previous study, we found that Osh3-GFP targeting to the cER was impaired in *scs2*Δ *scs22*Δ double mutant cells (see Figure S3D). As expected, substitution of the FFAT motif in combination with deletion of the PH domain (GFP-Osh3$^{\Delta PH,\ AAAT}$) (Figure 2D) resulted in inactivation of Osh3 because this mutant protein did not rescue the growth defect of *osh*Δ:*CEN osh4*^{ts} cells (Figure 2D). Moreover, Osh3$^{\Delta PH,AAAT}$-GFP localized diffusely in the cytoplasm, and not at cortical patches (Figure S2C). Thus, Osh3 undergoes multiple interactions involving at least PI4P and the Scs2/Scs22 VAP proteins to assemble and function at PM/ER membrane contact sites.

The VAP Proteins Scs2 and Scs22 Regulate PI4P Metabolism

We then addressed if the ER membrane VAP proteins Scs2/Scs22 control Osh3 function and PI4P metabolism. Because FFAT motifs from OSBP and Osh proteins bind VAP proteins (Figure 3A) (Kaiser et al., 2005; Loewen et al., 2003), we specifically confirmed interactions for Osh3 and Scs2. A GST-Osh3 N-terminal fragment containing the FFAT motif (GST-Osh3$^{1–613}$) (Figure 3A) bound to glutathione-sepharose beads efficiently isolated an Scs2-3xHA fusion from solubilized cell extracts (Figure 3B). GST alone was unable to bind Scs2-3xHA (Figure 3B). We then tested if the VAP proteins Scs2/Scs22 impact PI4P metabolism. PI4P levels were elevated 2.9-fold above wild-type in *scs2*Δ *scs22*Δ double mutant cells, as assessed by ^{3}H-inositol labeling (Figure 3C and Table S3). The PI4P FLARE was also stabilized at the PM in *scs2*Δ *scs22*Δ double mutant cells, particularly in mother cells (the PI4P FLARE was also weakly observed at intracellular puncta) (Figure 3D). Thus, Osh3 and Scs2 interact, and the VAP proteins Scs2/Scs22 control PI4P levels at the PM.

We performed additional tests to address how the VAP proteins Scs2/Scs22 might control PI4P metabolism. Sac1-GFP localized to nuclear and cER membrane compartments in *scs2*Δ *scs22*Δ double mutant cells (Figure S3A). Steady-state expression of Sac1-GFP and Osh3-GFP was unaffected in *scs2*Δ *scs22*Δ mutant cells, compared to wild-type cells (Figures S3B and S3C). Thus, whereas Sac1, Osh3, and the VAP proteins Scs2/Scs22 act in common to control PI4P metabolism, the VAP proteins are not required for Sac1 or Osh3 stability. Similar to the cortical localization of Osh3^{AAAT}-GFP (Figure S2C), Osh3-GFP localized to cortical structures in *scs2*Δ *scs22*Δ mutant cells (Figure S3D). However, Osh3-GFP cortical patches did not appear to be associated with the peripheral ER in *scs2*Δ *scs22*Δ mutant cells (Figure S3D), consistent with a previous study (Loewen et al., 2003). These findings suggest that PI4P metabolism at PM/ER junctions may occur in regulated stages. Osh3 may initially assemble at the PM, possibly as a PI4P sensor via its PH domain. Subsequent interactions between Osh3 and the VAP proteins may lead to stimulation of Sac1 PI phosphatase activity at PM/ER junctions.

The Osh and VAP Proteins Control Sac1 Phosphatase Activity

To test if the VAP and Osh proteins regulate Sac1 activity, we set up an in vitro phosphatase assay using PI4P-containing liposomes (PC:PS:PI4P) and microsomes containing integral Sac1-GFP prepared from cellular membranes (Figures 4A; Figure S4A). PI4P phosphatase activity was readily detected with wild-type microsomes (145 pmol/μg total protein/min, at 10 min) (Figure 4A) and was specifically due to Sac1-GFP because microsomes prepared from *sac1*Δ cells lacked activity (Figure 4A). We also did not detect significant phosphatase activity using Sac1-GFP microsomal preps against liposomes lacking PI4P (PC:PS:PtdIns liposomes) (Figure S4B). Thus, this in vitro assay followed microsome-embedded Sac1 activity against PI4P presented on liposomes, rather than PI species that might be present in the microsomes.

To confirm that liposomes did not fuse with Sac1-GFP microsomes or that PI4P did not transfer from liposomes to microsomes, we incubated Sac1-GFP microsomes with liposomes containing ^{3}H-labeled PI4P and PI(4,5)P_2 (Figure S4C). Following a 30-min incubation at 37°C (the course of the phosphatase assays) (Figures 4A and Figure S4B), Sac1-GFP microsomes were immunoisolated using anti-GFP antibodies and protein A-coupled magnetic Dynabeads (Figure S4D). Unbound liposomes (and microsomes not containing Sac1-GFP) were subsequently sedimented by high-speed centrifugation. The amount of ^{3}H-PI species in isolated Sac1-GFP microsomes, sedimented liposomes, and the resulting supernatant fraction was determined by liquid scintillation counting. Only a minor portion, 3.1% ± 0.9% of the total ^{3}H-PI, associated with isolated Sac1-GFP microsomes (Figure S4E, bound fraction). The bulk of ^{3}H-PI, 93.1% ± 6.2%, was present in the unbound fraction (Figure S4E). Of ^{3}H-PI in the unbound fraction, 88.5% ± 1.3% sedimented upon high-speed centrifugation (Figure S4F, P100 fraction), indicating that the majority remained in a membrane bilayer. A small amount of the unbound fraction, 11.5% ± 1.2%, was found in the supernatant fraction, perhaps due to micelles that did not sediment (Figure S4F, S100 fraction). Thus, liposomes did not fuse with Sac1-GFP microsomes, and ^{3}H-PI species were not efficiently transferred from liposomes to Sac1-GFP microsomes, under conditions that resulted in efficient dephosphorylation of PI4P in liposomes (Figures 4A and Figure S4B). We also performed experiments in the presence of recombinant Osh3 (GST-Osh3$^{588–996}$ including the FFAT and ORD; see Figure 5A). However, the distribution of ^{3}H-PI species was not significantly affected by the addition of GST-Osh3$^{588–996}$ (Figures S4E and S4F). Similarly, purified his$_6$-Osh4 (Figure 5A) did not significantly alter the distribution of ^{3}H-PI species in analogous experiments (unpublished data). Thus, Osh3 and Osh4 did not enhance membrane fusion or ^{3}H-PI transfer between liposomes and Sac1-GFP microsomes.

Following these control experiments, we addressed whether the VAP proteins controlled Sac1 PI phosphatase activity. Microsomes lacking Scs2 and Scs22 were impaired in the initial rate of PI4P turnover (more than 2-fold: 66 pmol/μg total protein/min, at 10 min, as compared to wild-type) (Figure 4A). In addition, *scs2*Δ *scs22*Δ microsomes were impaired in maximal Sac1 phosphatase activity as compared to wild-type microsomes (1232 ± 159 pmol PO_4 released versus 2543 ± 274 pmol, respectively) (Figure 4A). Levels of Sac1-GFP and the ER protein Dpm1 were similar in both wild-type and *scs2*Δ *scs22*Δ microsomal preparations (Figure S4A). Thus, whereas Sac1-GFP levels

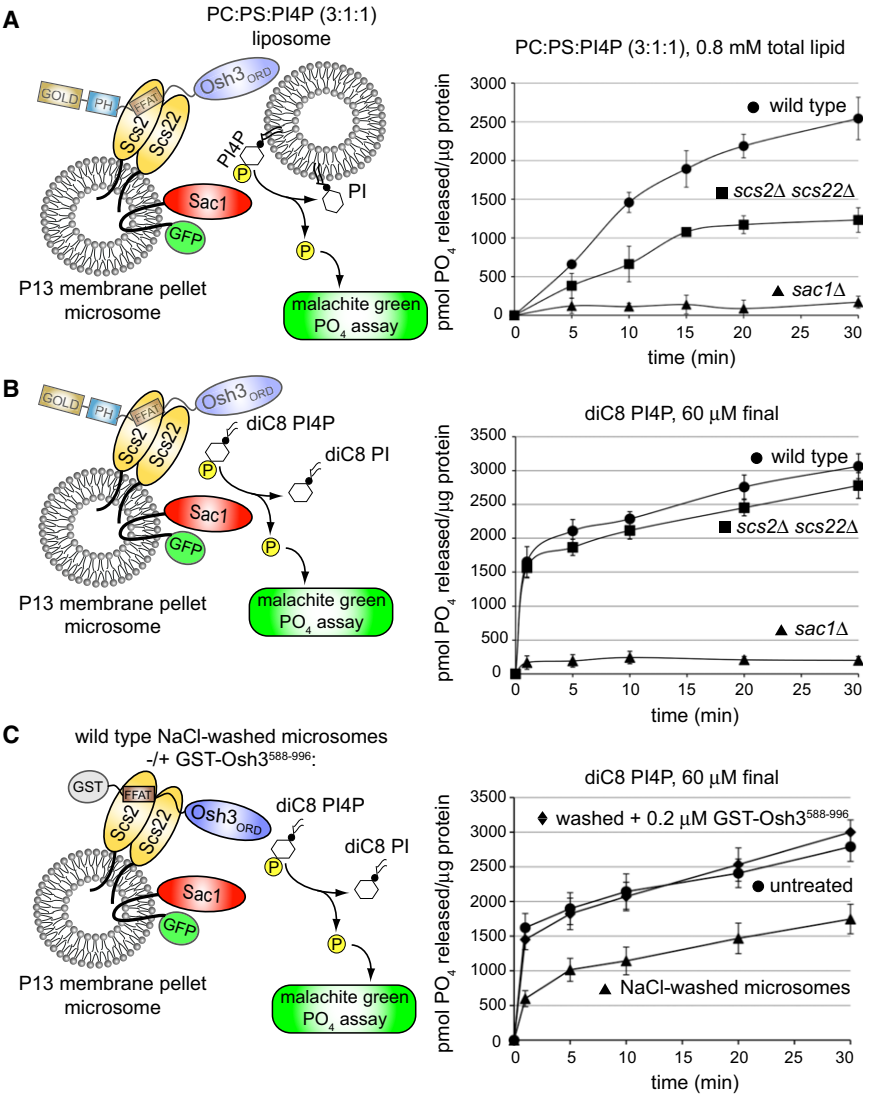

Figure 4. The VAP Proteins Scs2/Scs22 Control Sac1 PI Phosphatase Activity In Vitro

(A) PI4P-containing liposomes were incubated with wild-type (circles), *scs2*Δ *scs22*Δ (squares), or *sac1*Δ (triangles) microsomes for the indicated times. Phosphate release was measured by a malachite green assay. Error bars show the SD of two experiments measured in duplicate. See also Figure S4.

(B) Short acyl chain diC8 PI4P was incubated with wild-type (circles), *scs2*Δ *scs22*Δ (squares), or *sac1*Δ (triangles) microsomes for the indicated times. Error bars show the SD of two experiments measured in duplicate.

(C) Short acyl chain diC8 PI4P was incubated with untreated (circles), NaCl-washed (triangles), or NaCl-washed microsomes in the presence of GST-Osh3$^{588–996}$ (diamonds) for the indicated times. Error bars show the SD of two experiments measured in duplicate. See also Figure S5A.

were similar, Sac1 activity was impaired in *scs2*Δ *scs22*Δ microsomes. Importantly, to our knowledge, these experiments provide the first in vitro demonstration of Sac1 activity in *trans* and indicate that the yeast VAP proteins promote this activity.

Wild-type and *scs2*Δ *scs22*Δ microsomes demonstrated similar activity against a soluble substrate, short acyl chain diC8 PI4P (in the absence of other lipids) (Figure 4B), indicating that both microsomal preps contained similar intrinsic Sac1 activity. As in the PI4P liposome assay, microsomes isolated from *sac1*Δ cells did not display activity against diC8 PI4P (Figure 4B). Notably, both wild-type and *scs2*Δ *scs22*Δ microsomes displayed increased activity for the soluble diC8 PI4P substrate (approximately 1500 pmol PO_4 released/μg total protein/min, after 1 min) (Figure 4B). At later time points both preps continued to display similar turnover rates, although slower likely due to reduced substrate concentrations. Thus, the VAP proteins Scs2/Scs22 may act to link Sac1 to substrates on opposing membranes, possibly through the FFAT-containing Osh proteins, Osh2 and Osh3.

We then tested if the Osh proteins stimulate Sac1 activity in vitro. Because Sac1 levels were reduced in *osh*Δ:*CEN osh4*^{ts} cell lysates (Figure S1B and Figure S4A), we did not use microsomes prepared from these mutant cells. However, we found that Osh3 was depleted from membrane fractions by incubation in high salt (unpublished data). Sac1-GFP microsomes were then subjected to a high-salt wash to deplete peripherally associated membrane proteins, such as Osh3. Sac1-containing microsomes were not active against PI4P-containing liposomes following the high-salt wash. Thus, we were not able to test whether recombinant Osh3 stimulated Sac1 in *trans* activity (unpublished data). However, NaCl-washed microsomes displayed a reduced rate of diC8 PI4P turnover (more than 2-fold: 600 ± 115 pmol/μg total protein/min, after 1 min, as compared to untreated microsomes at 1600 ± 206 pmol/μg total protein/min, after 1 min) (Figure 4C) and maximal Sac1 phosphatase activity compared to untreated microsomes (1746 ± 213 pmol PO_4 released versus 2789 ± 211 pmol, respectively, after 30 min) (Figure 4C). To test if impaired Sac1 activity in NaCl-washed microsomes was due to the loss of Osh proteins, purified GST-Osh3$^{588–996}$ (see Figure 5B) was added back to the reaction. Strikingly, 0.2 μM GST-Osh3$^{588–996}$ restored activity in salt-washed microsomes to levels nearly identical to untreated Sac1-GFP microsomes (1450 ± 155 pmol/μg total protein/min after 1 min, and 3000 ± 176 pmol PO_4 released after 30 min) (Figure 4C). Thus, recombinant Osh3 stimulated full-length Sac1 in microsomes, providing the first evidence that ORPs control Sac1 PI phosphatase activity in vitro.

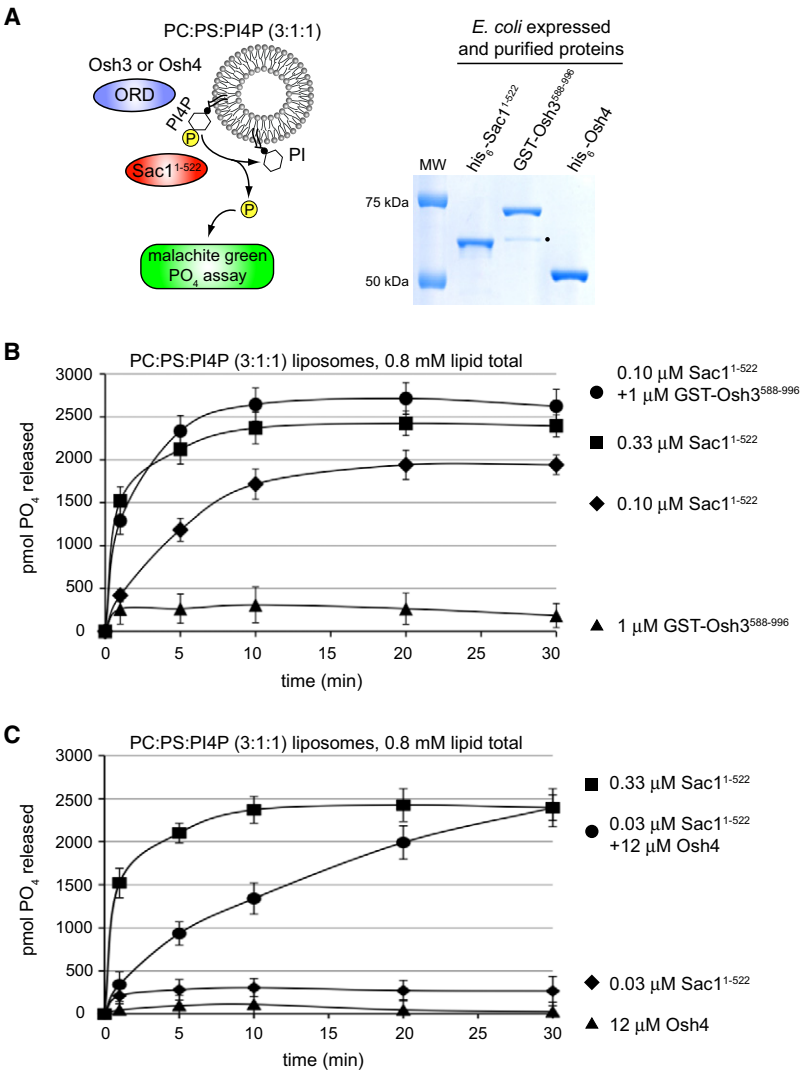

Figure 5. The ORDs Stimulate Sac1 Activity In Vitro

(A) Schematic of the reconstituted Sac1 phosphatase assay. PI4P-containing liposomes were incubated with his_6-$Sac1^{1–522}$, GST-$Osh3^{588–996}$ or his_6-Osh4. Phosphate release was measured by a malachite green assay. The Coomassie-stained gel shows the recombinant proteins used in the in vitro assays. The dot indicates a GST-$Osh3^{588–996}$ degradation product.

(B) GST-$Osh3^{588–996}$ stimulates Sac1 in vitro. Results from in vitro phosphatase assays including 0.33 μM his_6-$Sac1^{1–522}$ (squares), 0.1 μM his_6-$Sac1^{1–522}$ (diamonds), 1 μM GST-$Osh3^{588–996}$ and 0.1 μM $Sac1^{1–522}$ (circles), and background levels in the presence of 1 μM GST-$Osh3^{588–996}$ alone (triangles). Error bars show SD of two experiments measured in duplicate. See also Figure S5B.

(C) Osh4 stimulates Sac1 in vitro. Results from in vitro phosphatase assays with 0.33 μM his_6-$Sac1^{1–522}$ (squares), 0.03 μM his_6-$Sac1^{1–522}$ (diamonds), 0.03 μM his_6-$Sac1^{1–522}$ and 12 μM his_6-Osh4 (circles), and 12 μM his_6-Osh4 alone (triangles). Error bars show SD of two experiments measured in duplicate.

Reconstitution of Sac1 Phosphatase Activation by ORDs

Because the Osh3 ORD stimulated Sac1 activity in microsomes, we tested whether Osh proteins directly stimulate Sac1. We reconstituted Sac1 phosphatase activity in vitro using purified components at known concentrations. Sac1 lacking its transmembrane domains was expressed and purified from bacteria (his_6-$Sac1^{1–522}$) and incubated with PI4P-containing liposomes (Figure 5A). Purified his_6-$Sac1^{1–522}$ dephosphorylated PI4P in a dose and time-dependent manner (400 pmol/min/μg protein for 0.33 μM his_6-$Sac1^{1–522}$ after 5 min) (Figure 5B). At 0.1 μM his_6-$Sac1^{1–522}$, the turnover rate was reduced to approximately 250 pmol PO_4 released/min/μg protein after 5 min (Figures 5B and Figure S5D). A mutant form of Sac1 bearing substitutions in both cysteine residues in the CX_5R active site (his_6-$Sac1^{C392S,\ C395S}$) (Figure S5C) did not display phosphatase activity against PI4P-containing liposomes (Figure S5D). Importantly, addition of the Osh3 ORD (GST-$Osh3^{588–996}$) (Figure 5B) stimulated Sac1 phosphatase activity 3-fold against PI4P-containing liposomes, as 0.1 μM his_6-$Sac1^{1–522}$ in the presence of 1 μM GST-$Osh3^{600–996}$ displayed a turnover rate similar to 0.33 μM his_6-$Sac1^{1–522}$ (Figure 5B). As a control, 1 μM GST alone did not increase Sac1 activity (Figure S5D). GST-$Osh3^{588–996}$ did not catalyze PI4P turnover in the absence of his_6-$Sac1^{1–522}$ (Figure 5B) or in the presence of inactive his_6-$Sac1^{C392S,\ C395S}$ (Figure S5D).

Because the ORD is common to all ORPs, we addressed if Sac1 activation is a conserved function for the Osh proteins. We then tested if full-length Osh4/Kes1 stimulated Sac1 phosphatase activity in vitro. In these assays we lowered the his_6-$Sac1^{1–522}$ concentration (to 0.033 μM with activity near background levels) (Figure 5C). In the presence of 12 μM his_6-Osh4, 0.033 μM his_6-$Sac1^{1–522}$ activity increased 10-fold over

To test if GST-$Osh3^{588–996}$ required the VAP proteins to stimulate Sac1, Sac1-GFP microsomes prepared from *scs2*Δ *scs22*Δ mutant cells were washed with high salt to deplete peripheral membrane proteins. As expected, NaCl-washed *scs2*Δ *scs22*Δ microsomes displayed impaired rates of diC8 PI4P turnover, compared to untreated *scs2*Δ *scs22*Δ microsomes (more than 2-fold: 577 ± 151 pmol/μg total protein/min, after 1 min, as compared to untreated *scs2*Δ *scs22*Δ microsomes at 1315 ± 186 pmol/μg total protein/min, after 1 min) (Figure S5A). Salt-washed *scs2*Δ *scs22*Δ microsomes also displayed reduced maximal Sac1 phosphatase activity, compared to untreated *scs2*Δ *scs22*Δ microsomes (1364 ± 223 pmol PO_4 released versus 2652 ± 206 pmol, respectively, after 30 min) (Figure S5A). Interestingly, 0.2 μM GST-$Osh3^{588–996}$ restored full activity in salt-washed *scs2*Δ *scs22*Δ microsomes (1489 ± 145 pmol/μg total protein/min after 1 min, and 2994 ± 176 pmol PO_4 released after 30 min) (Figure S5A). Thus, the Osh3 ORD stimulated Sac1 activity against diC8 PI4P independently of the VAP proteins Scs2 and Scs22.

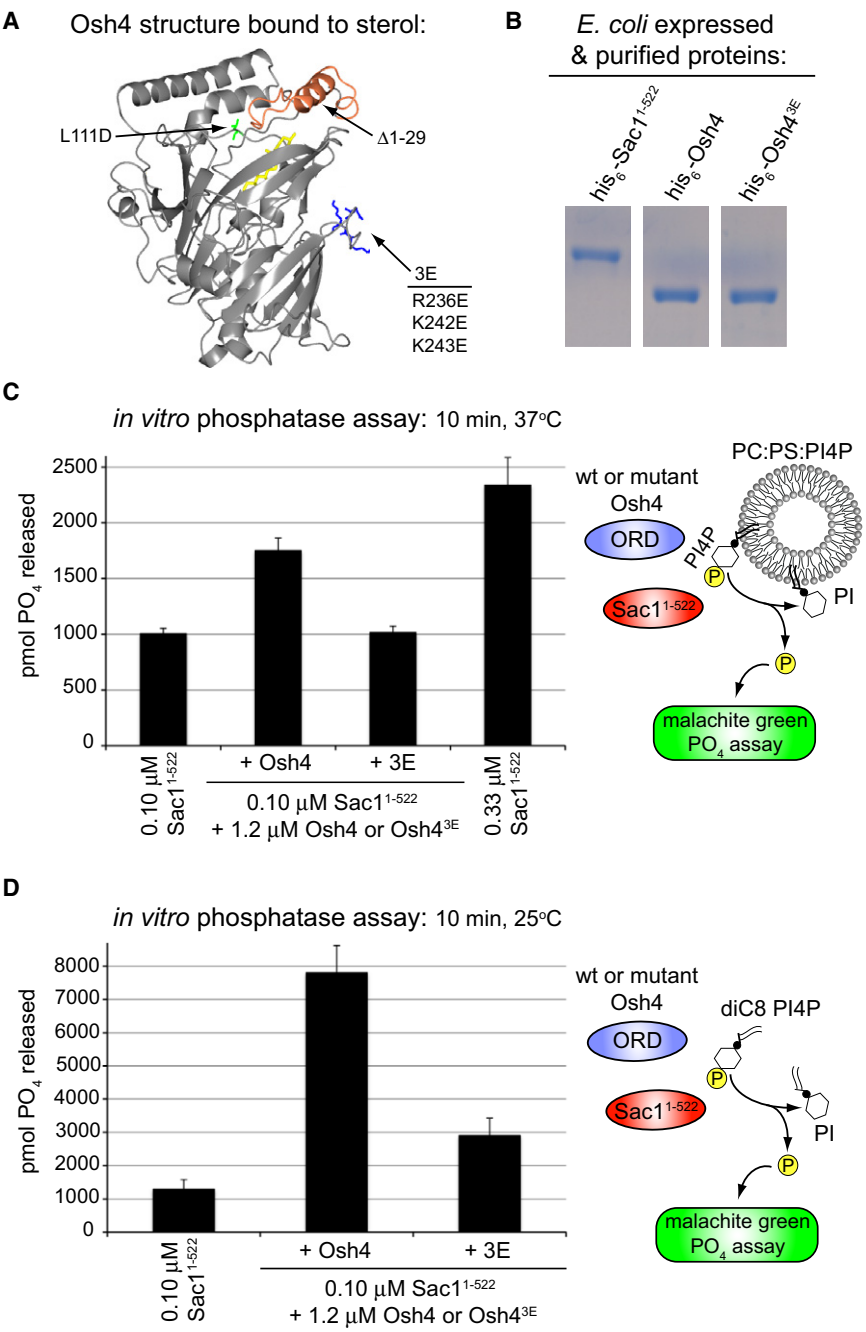

Figure 6. PI Binding Regulates Osh4 Function

(A) The structure of Osh4/Kes1 (Im et al., 2005) is shown with mutants used in this study. Osh4$^{\Delta 1-29}$ (orange) and Osh4^{L111D} (green) are defective in sterol binding (Im et al., 2005). Osh4^{3E} (R236E, R242E, R243E; blue) is impaired in PI binding (see Figures S6A and S6B) (Li et al., 2002). Cholesterol bound within the structure is shown in yellow.

(B) Coomassie-stained gel showing recombinant, purified his$_6$-Sac1$^{1-522}$ and wild-type and mutant his$_6$-Osh4 proteins.

(C) In vitro phosphatase assays using 0.1 μM his$_6$-Sac1$^{1-522}$ and wild-type and mutant Osh4^{3E} proteins (1.2 μM). PI4P liposomes (PC:PS:PI4P, 3:1:1) were tested. Error bars show the SD of two experiments each measured in duplicate.

(D) In vitro phosphatase assays using 0.1 μM his$_6$-Sac1$^{1-522}$ and wild-type and mutant Osh4^{3E} proteins (1.2 μM) against short acyl chain diC8 PI4P. Error bars show the SD of two experiments each measured in duplicate. See also Figure S6C.

the course of the experiment, reaching that of 0.33 μM his$_6$-Sac1$^{1-522}$ (Figure 5C). In addition, at high concentrations (300 μM) of short acyl chain diC8 PI4P, 1.2 μM his$_6$-Osh4 stimulated 0.1 μM his$_6$-Sac1$^{1-522}$ activity greater than 6-fold (Figures 6D and Figure S6C). Thus, the ORDs from Osh3 and Osh4 directly activated Sac1 in vitro.

PI and Sterol Binding Control Osh4 Function

Osh4/Kes1 binds PI lipids in vitro (Li et al., 2002). Consistent with this, his$_6$-Osh4 sedimented more efficiently with PI4P-containing liposomes, compared to phosphatidylinositol-containing liposomes (Figure S6A). GST-Osh3$^{588-996}$ also sedimented more readily with PI4P-containing liposomes than it did with PtdIns-containing liposomes (Figure S6A). We tested if PI binding was necessary for Osh4 function in vitro and in vivo. Substitution of three basic residues (R236E, K242E, K243E; termed 3E) (Figure 6A) impairs Osh4 PI binding (Li et al., 2002). The mutant his$_6$-Osh4^{3E} protein was stably expressed and purified (Figure 6B). We confirmed that his$_6$-Osh4^{3E} was defective in PI binding using an overlay assay (Figure S6B). In contrast, wild-type his$_6$-Osh4 bound PI3P, PI4P, and PI(4,5)P$_2$ (in order of binding affinity) (Figure S6B). Notably, his$_6$-Osh4^{3E} did not stimulate Sac1 activity against PI4P in liposomes (Figure 6C). In addition, his$_6$-Osh4^{3E} was impaired in Sac1 activation against short acyl chain diC8 PI4P, as compared to wild-type his$_6$-Osh4 (2-fold versus 6-fold stimulation, respectively) (Figure 6D). Consistent with these in vitro results, cellular PI4P levels were 17-fold above wild-type in *osh*Δ:*CEN osh4^{ts}* cells coexpressing Osh4^{3E} at 38°C (Table S3), indicating that PI binding is essential for Osh4 function.

Because the Osh proteins bind sterol lipids in vitro (Im et al., 2005; Raychaudhuri et al., 2006), we tested if sterol lipids regulate Osh-stimulated Sac1 activity. Addition of 250 μM cholesterol (>800-fold above the K_d of Osh4 for cholesterol) (Im et al., 2005) did not significantly affect Osh4-stimulated Sac1 activity against diC8 PI4P (Figure S6C). We also measured in vivo PI levels in *osh*Δ:*CEN osh4^{ts}* cells coexpressing wild-type *OSH4* or the

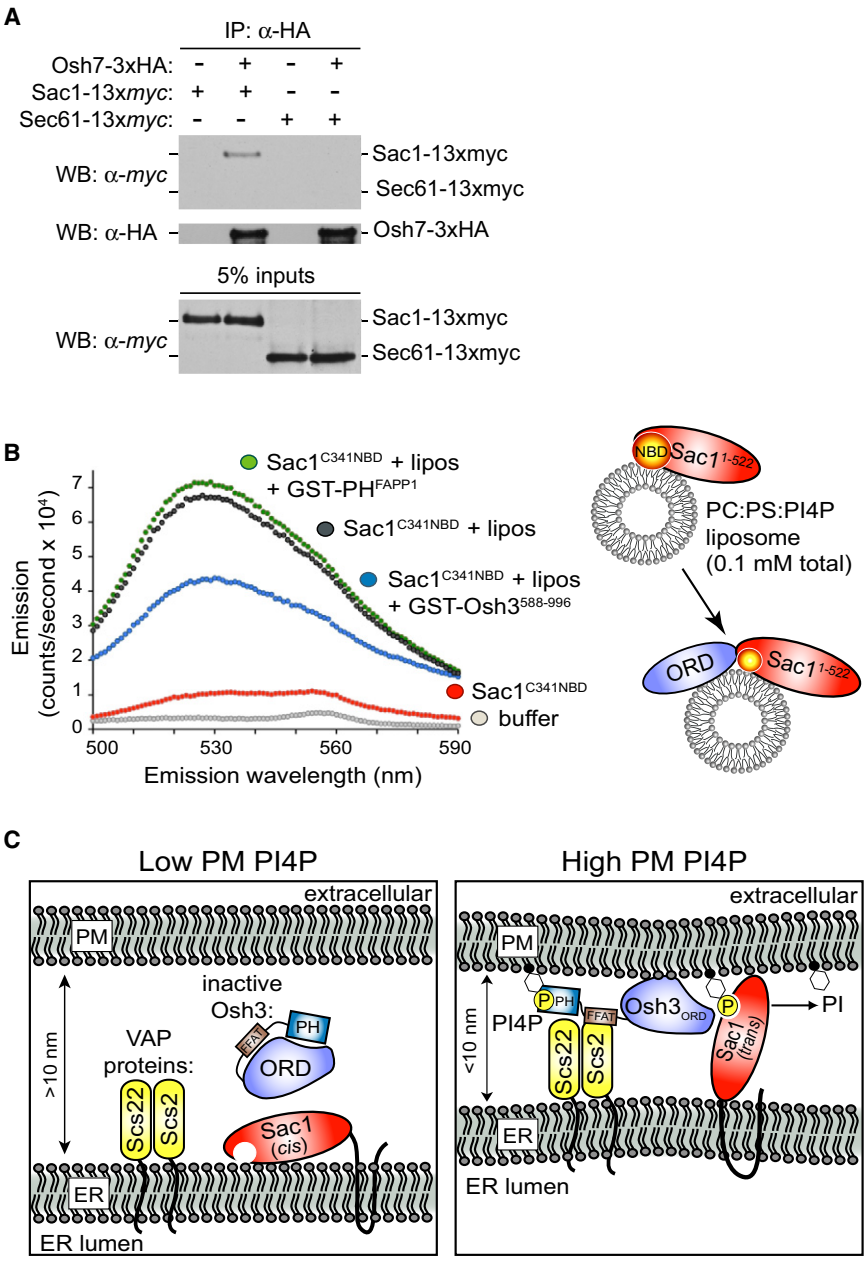

Figure 7. The ORD Interacts with Sac1 and Model for Regulation of PI4P Metabolism by Osh3, Scs2/Scs22, and Sac1 at PM/ER Membrane Contact Sites

(A) Sac1-13x*myc* specifically interacts with Osh7-3xHA. Membrane fractions from cells expressing Osh7-3xHA and Sac1-13x*myc* or Sec61-13x*myc* were incubated with cross-linkers, solubilized, immunoprecipitated with anti-HA beads, and analyzed by immunoblotting to detect Osh7-Sac1 complexes. See also Figure S7A.

(B) GST-Osh3$^{588–996}$ induces a conformational shift in the Sac1 catalytic domain. Emission scans of 0.06 μM Sac1^{C341NBD} in buffer (red), in the presence of liposomes (PC:PS:PI4P, 3:1:1, 0.1 mM lipid total; dark gray), liposomes and 0.8 μM GST-Osh3$^{588–996}$ (blue), liposomes with 0.8 μM GST-PH^{FAPP1} (green), and buffer alone (light gray). See also Figure S7.

(C) Model for PI4P turnover at PM/ER membrane contact sites. High PM PI4P levels recruit and activate Osh3 at ER/PM contact sites. Interactions between Osh3 and the VAP proteins Scs2/Sc22 activate ER-localized Sac1.

sterol-binding defective mutants, *osh4Δ1-29* or *osh4L111D* (see Figure 6A) (Im et al., 2005). In *oshΔ:CEN osh4^{ts}* cells coexpressing either Osh4$^{Δ1–29}$ or Osh4^{L111D}, PI4P levels were 21- and 19-fold above wild-type levels (Table S3). Thus, whereas cholesterol did not alter Sac1 activity in vitro, sterol binding was essential for Osh4-mediated PI4P metabolism in vivo.

The Osh Proteins Interact with the Sac1 Catalytic Domain

Because the Osh3 and Osh4 ORDs activated Sac1 in vitro, we examined if Osh proteins interact with Sac1. We initially used Osh7 for these experiments because it is expressed at higher levels than Osh3 (2350 Osh7 molecules/cell versus 600 Osh3 molecules/cell) (Ghaemmaghami et al., 2003). Osh7 localizes to the cER even though it lacks a PH domain and FFAT motif (Schulz et al., 2009) (Figure 1C). A membrane pellet fraction containing Osh7-3xHA and Sac1-13x*myc* was incubated with cross-linkers, solubilized, and processed for co-immunoprecipitation against the 3xHA tag on Osh7. A small fraction of Sac1-13x*myc* specifically isolated with Osh7-3xHA (Figure 7A), suggesting that this interaction was transient or possibly indirect because it required crosslinking. However, Sac1 is far more abundant in cells than Osh7 (48,000 Sac1 molecules/cell) (Ghaemmaghami et al., 2003); thus, only a small fraction of Sac1 is expected to co-isolate with Osh7. Importantly, Osh7-3xHA did not crosslink to another abundant ER membrane protein, Sec61-13x*myc* (Figure 7A). We also observed crosslinking between 3xHA-Osh3 and Sac1-13x*myc* (Figure S7A). As a control the ER transmembrane protein Wbp1 was not isolated with 3xHA-Osh3 (unpublished data). Together, these results suggested that multiple Osh proteins interact with Sac1 and that the ORD is responsible.

Next, we tested if the ORD and Sac1 domains physically interact in vitro. We were unable to detect a stable complex between the purified Sac1 domain and Osh3 or Osh4 ORDs in solution (unpublished data). For this reason we developed assays to monitor Sac1 and ORD interactions on a membrane bilayer. The Sac1$^{1–522}$ domain contains three

cysteine residues: C392 and C395 in the catalytic site and C341 in loop 4 (L4) that resides on the same surface as the catalytic site (Figure S7B) (Manford et al., 2010). Purified his_6-Sac1$^{C392S, C395S}$ was covalently labeled with the fluorescent dye NBD at C341 (Sac1^{C341NBD}) (Figure S7B). Movement of NBD from an aqueous environment to a more hydrophobic environment is accompanied by changes in its spectral properties (e.g., emission wavelength maximum, termed "blue shift," and intensity) and, thus, can be used as an indicator for conformational changes in a protein as well as membrane association. Sac1^{C341NBD} underwent a significant increase in NBD fluorescence signal (6.6-fold) and a shift in the maximum emission wavelength (blue shift) upon addition of liposomes (Figure 7B), reflecting a membrane-induced change in the local environment of L4 in the Sac1 catalytic domain. Interestingly, addition of GST-Osh3$^{588–996}$ reduced Sac1^{C341NBD} signal intensity in the presence of liposomes (1.7-fold), consistent with an Osh3-induced shift in L4 of Sac1 to a less hydrophobic environment (Figure 7B). As a control, GST fused to the PI4P-binding PH domain from FAPP1 did not alter the Sac1^{C341NBD} fluorescence signal in the presence of liposomes (Figure 7B). Thus, the Osh3 ORD-induced reduction in Sac1^{C341NBD} signal intensity was not simply due to competition for PI4P binding.

To address whether these effects were conferred by another ORD, we incubated Sac1^{C341NBD} with liposomes either in the absence or presence of his_6-Osh4. Addition of his_6-Osh4 reduced Sac1^{C341NBD} signal intensity in the presence of liposomes (1.7-fold) (Figure S7C), similar to GST-Osh3$^{588–996}$. Interestingly, the Osh4^{3E} mutant protein that is defective in PI binding and Sac1 stimulation did not affect Sac1^{C341NBD} fluorescence intensity in the presence of liposomes (Figure S7C). Because a change in NBD fluorescence can be due to effects in membrane association as well as protein conformational states, we examined the membrane-binding status of Sac1^{C341NBD} in the absence and presence of Osh4. Surprisingly, the ability of his_6-Sac1^{C341NBD} to sediment with liposomes was increased in the presence of his_6-Osh4 (>2-fold) (Figure S7D). Thus, the reduction in Sac1^{C341NBD} fluorescence intensity by Osh4 was not due to decreased Sac1 domain membrane binding. Accordingly, the Osh-induced shift in Sac1^{C341NBD} fluorescence intensity may reflect an Osh-induced conformational change in the Sac1 catalytic domain, consistent with Osh-stimulated Sac1 phosphatase activity in vitro. Moreover, an Osh-induced increase in membrane association may contribute to Sac1 activation.

DISCUSSION

Sac1-like phosphatases are essential regulators of PI-signaling networks. We show that the Osh proteins control Sac1 activity. Members of the ORP family are known to bind sterol and PI lipids and are implicated in disease (Ngo et al., 2010). We demonstrate a new role for this family: control of PI4P metabolism through Sac1 PI phosphatases. Our results also explain how ER-localized Sac1 can regulate PM PI4P levels in *trans*: via the function of Osh proteins at PM/ER membrane contact sites as sensors of PI4P at the PM and activators of the Sac1 phosphatase in the ER.

PM PI4P Metabolism Occurs at PM/ER Membrane Contact Sites

Recent studies have proposed that Sac1 regulates PI4P in *cis* at the ER and Golgi, as well as in *trans* at the PM from the ER (Baird et al., 2008; Manford et al., 2010). In accord, Sac1 has been shown to regulate PI4P levels at the ER and Golgi (Faulhammer et al., 2007; Foti et al., 2001). Our findings and additional evidence indicate that ER-localized Sac1 controls PM PI4P pools. First, PI4P accumulates at the PM in cells lacking Sac1 (Figure 1E) (Roy and Levine, 2004). Second, Sac1 does not traffic to the PM and was not stabilized at the PM in an endocytosis mutant (Tahirovic et al., 2005). Likewise, cells expressing a form of Sac1 that is retained in the ER do not display elevated PI4P levels (Konrad et al., 2002). Last, we demonstrate that full-length Sac1 in microsomes dephosphorylates PI4P in *trans* on distinct liposomes (Figure 4).

We propose that the Osh and VAP proteins function as regulators of Sac1 activity at membrane contact sites. Notably, Osh3 localization to PM/ER membrane sites was dependent on PI4P synthesis (Figure 2C), and a mutant form lacking the PH domain was destabilized from cortical patches (Figure S2C). We suggest that the PH domain-containing protein Osh3 acts as a sensor of PI4P levels at the PM and subsequently activates the Sac1 PI phosphatase at the ER (Figure 7C). Our study also highlights a role for Scs2 and Scs22 in PI4P metabolism. Cells lacking Scs2 and Scs22 display elevated PM PI4P levels (Figure 3). Moreover, Scs2 and Scs22 stimulate Sac1 activity against PI4P in liposomes (Figure 4A). Scs2 and Scs22 may activate Osh3 at PM/ER membrane contact sites to control PM PI4P levels (Figure 7C). The yeast VAP proteins may also aid in the formation of membrane junctions. Scs2 and Scs22 have been implicated in PM/ER membrane contact site formation (Loewen et al., 2007). In addition, Scs2 binds anionic phospholipids, including PI4P, in vitro (Kagiwada and Hashimoto, 2007).

Mechanisms for Regulation of Sac1 Activity by the Osh Proteins

Multiple inputs control Osh protein function. We propose that PI4P binding to the Osh3 PH domain and Scs2 interactions via the FFAT motif activate Osh3 at PM/ER membrane contact sites (Figure 7C). These interactions may then facilitate interactions between the Osh3 ORD and downstream target proteins such as Sac1 (Figure 7C). Thus, Osh3 may serve as a "co-incidence detector" of PI4P, the VAP proteins, and Sac1. We also found that PI and sterol binding control Osh4/Kes1 function (Figure 6; Table S3). The Osh proteins control sterol localization in vivo (Beh and Rine, 2004) and transfer sterol lipids in vitro (Raychaudhuri et al., 2006). Osh4/Kes1 function required sterol binding in vivo (Table S3) but was not affected by the addition of cholesterol in vitro (Figure S6C). The concentrations of Osh4 or PI4P in our in vitro studies may have bypassed a requirement for sterol binding. In vivo, the ability of the Osh proteins to extract sterol lipids may control membrane bilayer rigidity and curvature, and thus, formation of membrane contact sites (Figure 7C). Notably, the Osh proteins can tether liposomes in vitro (Schulz et al., 2009). Alternatively, sterol binding may control Osh protein localization in vivo. Consistent with this idea, OSBP localizes to the

ER when bound to cholesterol and to the Golgi when bound to 25-hydroxycholesterol (Peretti et al., 2008).

Osh4/Kes1 also binds PI lipids in vitro (Figure S6;) (Li et al., 2002). This may be a general feature of ORDs because the Osh3 ORD showed increased affinity for PI4P liposomes (Figure S6). A form of Osh4 impaired in PI binding (Figure S6) did not stimulate Sac1 activity in vitro (Figure 6). Although our results did not indicate that Osh3 transfers PI lipids (Figure S4), the Osh proteins may bind PI lipids and present substrates to Sac1 at the membrane interface. Alternatively, PI binding may be necessary for productive interactions with Sac1. This idea is supported by our findings that Osh3 and Osh4 induced changes in $Sac1^{C341NBD}$ spectral properties in the presence of liposomes, but PI binding-defective $Osh4^{3E}$ was incapable of interacting with Sac1 (Figures 7 and Figure S7). The Osh-induced effects on $Sac1^{C341NBD}$ signal intensity may reflect a conformational change in Sac1 or a shift in the orientation of Sac1 with respect to the membrane bilayer. In addition PI binding may be necessary for Osh-stimulated Sac1 membrane association (Figure S7D).

Conserved Functions for the Osh/ORP and VAP Proteins in PI Metabolism

ORP and VAP proteins may share conserved roles in PI homeostasis. Each of the Osh proteins partially rescues the PI4P metabolism defects in *osh*Δ:*CEN osh4*^{ts} cells (unpublished data). Both Osh3 and Osh4 stimulate Sac1 PI phosphatase activity in vitro (Figure 4, Figure 5, and Figure 6). Osh6 and Osh7 localize to the peripheral ER (Schulz et al., 2009), and Osh7 interacts with Sac1 in crosslinking experiments (Figure 7A). Osh1 localizes to nuclear-vacuole junctions to participate in lipid metabolism (Levine and Munro, 2001). Osh4 regulates PI4P at the Golgi (Fairn et al., 2007; Li et al., 2002) where it may regulate Sac1 activity. Likewise, mammalian ORP and VAP proteins have been implicated at membrane contact sites. A recent study found ORP1L and VAP at ER/endosome membrane contact sites (Rocha et al., 2009). Mammalian VAP proteins control PI4P metabolism at ER/Golgi membrane contact sites (Peretti et al., 2008). In addition, bound to 25-hydroxycholesterol, OSBP localizes to the Golgi and ER/Golgi contact sites (Peretti et al., 2008).

ORP and VAP proteins may regulate additional PI signaling networks. Osh7 and Scs2 overexpression rescued the growth defects of mutant yeast cells with toxic PI3P levels due to loss of the Sac1-like PI phosphatases Ymr1 and Sjl3, myotubularin and synaptojanin orthologs (Parrish et al., 2005). Cells lacking Osh or VAP protein function also display increased cellular PI3P levels (Table S3). It is unclear which Osh proteins regulate PI3P metabolism and if Osh and VAP proteins regulate other Sac1-like PI phosphatases, such as synaptojanins or myotubularin. Yet, cells lacking Osh function accumulate PI4P levels similar to *sac1 sjl2 sjl3* triple mutant cells (Figure 1) (Foti et al., 2001), suggesting that they may control Sac1-like activity encoded by the yeast synaptojanins.

We propose that the Osh proteins act as sensors of PI levels and regulate the Sac1 PI phosphatase at membrane contact sites. By retaining Sac1 at the ER, cells can recruit Sac1 to distinct organelle contact sites as needed (e.g., ER/PM, ER/Golgi, ER/endosome, ER/lysosome). This would allow the cell to maintain a wide range of Sac1 phosphatase activity and permit use of a common phosphatase (Sac1) to regulate PI lipids at multiple sites in the cell. Membrane contact sites facilitate communication between organelles through lipid transfer and metabolism (Lev, 2010). This elegant system may allow cells to balance not only PI levels but also other lipids at ER membrane contact sites because the ER is a major site of lipid synthesis. Thus, modulation of PI levels by Sac1, the Osh proteins, and VAP proteins may allow signaling between the ER and compartments along the secretory and endocytic systems, thus linking ER lipid biosynthesis to multiple membrane compartments in the cell. Interestingly, both Sac1 and the yeast VAP protein Scs2 are implicated in phospholipid metabolism (Loewen et al., 2004; Rivas et al., 1999). In addition, Sac1 has recently been identified as a component of a protein complex at the ER involved in sphingolipid metabolism (Breslow et al., 2010). Thus, future studies on Sac1 may reveal new insights into the links between membrane homeostasis and PI-signaling pathways.

EXPERIMENTAL PROCEDURES

Additional details of the Experimental Procedures are provided in the Extended Experimental Procedures.

Yeast Strains, Plasmids, and Media

Descriptions of strains and plasmids used in this study are in Table S1 and Table S2. Gene deletions and epitope tags were introduced by homologous recombination. Standard techniques were used for yeast and bacterial growth. Expression of recombinant proteins in bacteria is described in the Extended Experimental Procedures.

Fluorescence Microscopy

Microscopy was performed on mid-log cultures at the indicated temperatures. Images were obtained with a DeltaVision system equipped with an Olympus microscope, a 100× objective, and a Cool Snap HQ digital camera. Images were deconvolved with softWoRx 3.5.0 software. All results are based on observations of >100 cells.

PI Analysis

Cellular PI levels were measured as described (Baird et al., 2008). Additional details are in the Extended Experimental Procedures.

Protein Expression Levels

Cells incubated at the indicated temperatures were harvested, lysed, and the resulting extracts analyzed by SDS-PAGE and immunoblotting with the following antibodies: α-Myc (9E10), α-HA (12CA5), α-Pep12, α-Dpm1, and α-GFP.

Protein-Binding Assays

For Scs2-3xHA and GST-$Osh3^{1–613}$ binding, GST or GST-$Osh3^{1–613}$ immobilized on glutathione sepharose 4B was incubated with Scs2-3xHA lysates solubilized in PBS containing 0.5% Tween 20, 0.1 mM EDTA, and protease inhibitors. Beads were washed and analyzed by SDS-PAGE and immunoblotting. For Sac1-13x*myc* crosslinking to 3xHA-Osh3 and Osh7-3xHA, membrane fractions were incubated with 2 mM DSP and DTBP. Complexes were immunoisolated, reduced to cleave cross-linkers, and analyzed by SDS-PAGE and immunoblotting.

Sac1 Phosphatase Assays

For microsome assays, membrane fractions were sonicated in 50 mM Tris (pH 6.8), 150 mM NaCl, 2 mM DTT, 1 mM EDTA to form microsomes.

Liposomes (0.6 mM PC:0.2 mM PS:0.2 mM PI4P) were prepared by sonicating hydrated lipids in reaction buffer (50 mM Tris [pH 6.8], 150 mM NaCl, 2 mM DTT). Microsomes were incubated with liposomes or diC8 PI4P, and reactions were stopped with 50 mM *N*-ethylmaleimide (NEM). Phosphate release was measured by the addition of Biomol Green and measured at OD_{620}.

For assays with recombinant $Sac1^{1-522}$ and Osh proteins, proteins were added at indicated concentrations to liposomes or diC8 PI4P in reaction buffer at the indicated temperatures. Cholesterol-containing liposomes (0.6 mM PC:0.2 mM PS:0.2 mM PI4P:0.2 mM cholesterol) were prepared as described above. Reactions were stopped at the indicated times with NEM, and phosphate release was assayed as described above.

Lipid-Binding Assays

For overlay assays, lipids solubilized in chloroform:methanol were spotted onto nitrocellulose as indicated. Membranes were incubated overnight with purified proteins. Membranes were washed, and bound protein was detected by immunoblotting. For liposome sedimentation, liposomes were prepared as described, incubated with purified recombinant proteins, and centrifuged at 100,000 × g. The supernatant and pellet fractions were resolved by SDS-PAGE, and proteins were detected by Coomassie staining.

NBD Protein Labeling and Fluorescence Spectroscopy

Purified his_6-$Sac1^{C392S,C395S}$ labeled with IANBD [*N,N′*-dimethyl-*N*-(iodoacetyl)-*N′*-(7-nitrobenz-2-oxa-1,3-diazolyl)ethylenediamine] was dialyzed to remove excess IANBD. See the Extended Experimental Procedures for further details on fluorescence spectroscopy.

SUPPLEMENTAL INFORMATION

Supplemental Information includes Extended Experimental Procedures, seven figures, and three tables and can be found with this article online at doi:10.1016/j.cell.2010.12.034.

ACKNOWLEDGMENTS

We thank C. Beh for strains and plasmids. We are grateful to S. Weys for technical assistance. We thank members of the S.D.E. laboratory, C. McMaster, and S. Henry for discussions, and A. Bretscher, C. Fromme, and D. Teis for comments on the manuscript. This work was supported by funds from the Weill Institute for Cell and Molecular Biology (S.D.E.).

Received: June 2, 2010
Revised: September 17, 2010
Accepted: December 10, 2010
Published: February 3, 2011

REFERENCES

Audhya, A., Foti, M., and Emr, S.D. (2000). Distinct roles for the yeast phosphatidylinositol 4-kinases, Stt4p and Pik1p, in secretion, cell growth, and organelle membrane dynamics. Mol. Biol. Cell *11*, 2673–2689.

Baird, D., Stefan, C., Audhya, A., Weys, S., and Emr, S.D. (2008). Assembly of the PtdIns 4-kinase Stt4 complex at the plasma membrane requires Ypp1 and Efr3. J. Cell Biol. *183*, 1061–1074.

Beh, C.T., and Rine, J. (2004). A role for yeast oxysterol-binding protein homologs in endocytosis and in the maintenance of intracellular sterol-lipid distribution. J. Cell Sci. *117*, 2983–2996.

Blagoveshchenskaya, A., Cheong, F.Y., Rohde, H.M., Glover, G., Knodler, A., Nicolson, T., Boehmelt, G., and Mayinger, P. (2008). Integration of Golgi trafficking and growth factor signaling by the lipid phosphatase SAC1. J. Cell Biol. *180*, 803–812.

Breslow, D.K., Collins, S.R., Bodenmiller, B., Aebersold, R., Simons, K., Shevchenko, A., Ejsing, C.S., and Weissman, J.S. (2010). Orm family proteins mediate sphingolipid homeostasis. Nature *463*, 1048–1053.

D'Angelo, G., Vicinanza, M., Di Campli, A., and De Matteis, M.A. (2008). The multiple roles of PtdIns(4)P–not just the precursor of PtdIns(4,5)P2. J. Cell Sci. *121*, 1955–1963.

Fairn, G.D., Curwin, A.J., Stefan, C.J., and McMaster, C.R. (2007). The oxysterol binding protein Kes1p regulates Golgi apparatus phosphatidylinositol-4-phosphate function. Proc. Natl. Acad. Sci. USA *104*, 15352–15357.

Faulhammer, F., Kanjilal-Kolar, S., Knodler, A., Lo, J., Lee, Y., Konrad, G., and Mayinger, P. (2007). Growth control of Golgi phosphoinositides by reciprocal localization of sac1 lipid phosphatase and pik1 4-kinase. Traffic *8*, 1554–1567.

Foti, M., Audhya, A., and Emr, S.D. (2001). Sac1 lipid phosphatase and Stt4 phosphatidylinositol 4-kinase regulate a pool of phosphatidylinositol 4-phosphate that functions in the control of the actin cytoskeleton and vacuole morphology. Mol. Biol. Cell *12*, 2396–2411.

Ghaemmaghami, S., Huh, W.K., Bower, K., Howson, R.W., Belle, A., Dephoure, N., O'Shea, E.K., and Weissman, J.S. (2003). Global analysis of protein expression in yeast. Nature *425*, 737–741.

Guo, S., Stolz, L.E., Lemrow, S.M., and York, J.D. (1999). SAC1-like domains of yeast SAC1, INP52, and INP53 and of human synaptojanin encode polyphosphoinositide phosphatases. J. Biol. Chem. *274*, 12990–12995.

Im, Y.J., Raychaudhuri, S., Prinz, W.A., and Hurley, J.H. (2005). Structural mechanism for sterol sensing and transport by OSBP-related proteins. Nature *437*, 154–158.

Kagiwada, S., and Hashimoto, M. (2007). The yeast VAP homolog Scs2p has a phosphoinositide-binding ability that is correlated with its activity. Biochem. Biophys. Res. Commun. *364*, 870–876.

Kaiser, S.E., Brickner, J.H., Reilein, A.R., Fenn, T.D., Walter, P., and Brunger, A.T. (2005). Structural basis of FFAT motif-mediated ER targeting. Structure *13*, 1035–1045.

Konrad, G., Schlecker, T., Faulhammer, F., and Mayinger, P. (2002). Retention of the yeast Sac1p phosphatase in the endoplasmic reticulum causes distinct changes in cellular phosphoinositide levels and stimulates microsomal ATP transport. J. Biol. Chem. *277*, 10547–10554.

Lev, S. (2010). Non-vesicular lipid transport by lipid-transfer proteins and beyond. Nat. Rev. Mol. Cell Biol. *11*, 739–750.

Levine, T.P., and Munro, S. (2001). Dual targeting of Osh1p, a yeast homologue of oxysterol-binding protein, to both the Golgi and the nucleus-vacuole junction. Mol. Biol. Cell *12*, 1633–1644.

Li, X., Rivas, M.P., Fang, M., Marchena, J., Mehrotra, B., Chaudhary, A., Feng, L., Prestwich, G.D., and Bankaitis, V.A. (2002). Analysis of oxysterol binding protein homologue Kes1p function in regulation of Sec14p-dependent protein transport from the yeast Golgi complex. J. Cell Biol. *157*, 63–77.

Liu, Y., and Bankaitis, V.A. (2010). Phosphoinositide phosphatases in cell biology and disease. Prog. Lipid Res. *49*, 201–217.

Liu, Y., Boukhelifa, M., Tribble, E., Morin-Kensicki, E., Uetrecht, A., Bear, J.E., and Bankaitis, V.A. (2008). The Sac1 phosphoinositide phosphatase regulates Golgi membrane morphology and mitotic spindle organization in mammals. Mol. Biol. Cell *19*, 3080–3096.

Loewen, C.J., Roy, A., and Levine, T.P. (2003). A conserved ER targeting motif in three families of lipid binding proteins and in Opi1p binds VAP. EMBO J. *22*, 2025–2035.

Loewen, C.J., Gaspar, M.L., Jesch, S.A., Delon, C., Ktistakis, N.T., Henry, S.A., and Levine, T.P. (2004). Phospholipid metabolism regulated by a transcription factor sensing phosphatidic acid. Science *304*, 1644–1647.

Loewen, C.J., Young, B.P., Tavassoli, S., and Levine, T.P. (2007). Inheritance of cortical ER in yeast is required for normal septin organization. J. Cell Biol. *179*, 467–483.

Manford, A., Xia, T., Saxena, A.K., Stefan, C., Hu, F., Emr, S.D., and Mao, Y. (2010). Crystal structure of the yeast Sac1: implications for its phosphoinositide phosphatase function. EMBO J. *29*, 1489–1498.

Nemoto, Y., Kearns, B.G., Wenk, M.R., Chen, H., Mori, K., Alb, J.G., Jr., De Camilli, P., and Bankaitis, V.A. (2000). Functional characterization of a mammalian Sac1 and mutants exhibiting substrate-specific defects in phosphoinositide phosphatase activity. J. Biol. Chem. *275*, 34293–34305.

Ngo, M.H., Colbourne, T.R., and Ridgway, N.D. (2010). Functional implications of sterol transport by the oxysterol-binding protein gene family. Biochem. J. *429*, 13–24.

Parrish, W.R., Stefan, C.J., and Emr, S.D. (2005). PtdIns(3)P accumulation in triple lipid-phosphatase-deletion mutants triggers lethal hyperactivation of the Rho1p/Pkc1p cell-integrity MAP kinase pathway. J. Cell Sci. *118*, 5589–5601.

Peretti, D., Dahan, N., Shimoni, E., Hirschberg, K., and Lev, S. (2008). Coordinated lipid transfer between the endoplasmic reticulum and the Golgi complex requires the VAP proteins and is essential for Golgi-mediated transport. Mol. Biol. Cell *19*, 3871–3884.

Raychaudhuri, S., Im, Y.J., Hurley, J.H., and Prinz, W.A. (2006). Nonvesicular sterol movement from plasma membrane to ER requires oxysterol-binding protein-related proteins and phosphoinositides. J. Cell Biol. *173*, 107–119.

Rivas, M.P., Kearns, B.G., Xie, Z., Guo, S., Sekar, M.C., Hosaka, K., Kagiwada, S., York, J.D., and Bankaitis, V.A. (1999). Pleiotropic alterations in lipid metabolism in yeast sac1 mutants: relationship to "bypass Sec14p" and inositol auxotrophy. Mol. Biol. Cell *10*, 2235–2250.

Roy, A., and Levine, T.P. (2004). Multiple pools of phosphatidylinositol 4-phosphate detected using the pleckstrin homology domain of Osh2p. J. Biol. Chem. *279*, 44683–44689.

Schulz, T.A., Choi, M.G., Raychaudhuri, S., Mears, J.A., Ghirlando, R., Hinshaw, J.E., and Prinz, W.A. (2009). Lipid-regulated sterol transfer between closely apposed membranes by oxysterol-binding protein homologues. J. Cell Biol. *187*, 889–903.

Tahirovic, S., Schorr, M., and Mayinger, P. (2005). Regulation of intracellular phosphatidylinositol-4-phosphate by the Sac1 lipid phosphatase. Traffic *6*, 116–130.

Voeltz, G.K., Prinz, W.A., Shibata, Y., Rist, J.M., and Rapoport, T.A. (2006). A class of membrane proteins shaping the tubular endoplasmic reticulum. Cell *124*, 573–586.

Wei, H.C., Sanny, J., Shu, H., Baillie, D.L., Brill, J.A., Price, J.V., and Harden, N. (2003). The Sac1 lipid phosphatase regulates cell shape change and the JNK cascade during dorsal closure in Drosophila. Curr. Biol. *13*, 1882–1887.